Rheological State Diagrams for Rough Colloids in Shear Flow

Lilian C. Hsiao, Safa Jamali, Emmanouil Glynos, Peter F. Green, Ronald G. Larson, and Michael J. Solomon

Rheological state diagrams for rough colloids in shear flow

Lilian C. Hsiao[1,*,¶], Safa Jamali[2,¶], Daniel J. Beltran-Villegas[3], Emmanouil Glynos[4,§],

Peter F. Green[4], Ronald G. Larson[3] & Michael J. Solomon[3]

[1] Department of Chemical and Biomolecular Engineering, North Carolina State University, Raleigh, NC 27695, USA.

[2] Department of Chemical Engineering, Massachusetts Institute of Technology, Cambridge, MA 02139, USA.

[3] Department of Chemical Engineering, University of Michigan, Ann Arbor, MI 48109, USA.

[4] Department of Material Science and Engineering, University of Michigan, Ann Arbor, MI 48109, USA.

[§] Present address: Institute of Electronic Structure and Laser, Foundation for Research and Technology-Hellas, Crete, Greece.

[*] Corresponding author. e-mail: lilian_hsiao@ncsu.edu.

[¶] These authors contributed equally to this work.

1 **Abstract**

2   To assess the role of particle roughness in the rheological phenomena of
3 concentrated colloidal suspensions, we develop model colloids with varying surface
4 roughness length scales up to 10% of the particle radius. Increasing surface roughness
5 shifts the onset of both shear thickening and dilatancy towards lower volume fractions
6 and critical stresses. Experimental data are supported by computer simulations of
7 spherical colloids with adjustable friction coefficients, demonstrating that a reduction in
8 the onset stress of thickening and a sign change in the first normal stresses occurs when
9 friction competes with lubrication. In the quasi-Newtonian flow regime, roughness
10 increases the effective packing fraction of colloids. As the shear stress increases and
11 suspensions of rough colloids approach jamming, the first normal stresses switch signs
12 and the critical force required to generate contacts is drastically reduced. This is likely a
13 signature of the lubrication films giving way to roughness-induced tangential interactions
14 that bring about load-bearing contacts in the compression axis of flow.

15   Shear thickening is an increase in the viscosity, η, of a concentrated suspension of

16   particles in a fluid as the shear stress (σ) or shear rate rises beyond a critical value [1].

17   When suspensions shear thicken at high volume fractions, ϕ, it is frequently accompanied

18   by complex behavior that includes shear banding [2, 3] and slow stress decays [4]. The

19   degree of shear thickening can range from a few-fold to orders of magnitude increase in η

20   as a function of σ. These distinctions are typically used as working definitions for

21   continuous shear thickening (CST) and discontinuous shear thickening (DST) in the

22   literature [5]. We define weak and strong thickening using the power β as the slope of

23   log(η) plotted against log(σ) [6], where weak thickening occurs at $0.1 \leq \beta \leq 0.7$ and

24   strong thickening occurs at $0.7 < \beta \leq 1.0$. These categories are convenient classifications

25   of the magnitude of the rheological response rather than a fundamental physical

26   transition. Shifting the value of demarcation between weak and strong thickening has no

27   qualitative impact on the state diagrams presented.

28   Dilatancy is sometimes observed with strong shear thickening. Reynolds showed

29   that a dilatant suspension expands in volume because particles cannot otherwise find

30   direct flow paths within the confined environment [7]. This tendency to expand causes

31   the first normal stress difference, N_1, to switch from negative to positive values. The

32   onset stresses for shear thickening and dilatancy do not necessarily coincide [6, 8].

33   Similarly, a sheared suspension that freely expands in volume will not shear thicken

34   because of the lack of a confining stress [9, 10].

35   To date, neither hydrodynamics nor friction has successfully explained the full

36   range of flow phenomena in concentrated suspensions. When particles are pushed into

37   close contact at high shear rates, lubrication between the particles results in fore-aft

38 asymmetry and the subsequent formation of hydroclusters [11, 12]. A hallmark of the

39 asymmetric flow microstructure is the negative sign of N_1 [13-15], which has been

40 measured experimentally [13, 16, 17]. However, hydrodynamics theory alone cannot

41 explain the large viscosity increase in strong thickening or positive N_1 values at high σ

42 and ϕ. A recently proposed frictional contact model suggests that DST is a result of

43 particles making solid-solid contact when lubrication films break [2, 6, 18-23]. However,

44 numerical simulations of this model consistently predicts positive N_1 values regardless of

45 the flow conditions or the particle loading [24].

46   The reasons for discrepancies between theory, simulations, and experiments are

47 unclear, especially when particles are neither spherical nor smooth. In this Letter, we seek

48 to resolve these contradictions by systematically tuning the roughness of model colloids,

49 investigating their η and N_1 under shear, and demonstrating how surface roughness

50 influences the macroscopic response of the suspension. Here, a rough particle has

51 spherical symmetry and surface topography that deviates from an ideal smooth sphere by

52 <10% of the radius. Few studies relate particle surface roughness to frictional effects in

53 flow. One such study investigated the rheology of smooth and etched silica particles in a

54 narrow range of volume fractions ($0.41 \leq \phi \leq 0.48$) [25]. The authors found that the onset

55 stress for suspensions of etched silica is reduced when compared to smooth particles, and

56 that N_1 switches signs from negative to positive. Although this result is in qualitative

57 agreement with our work, their measured viscosities were higher than expected for near

58 hard sphere silica colloids [26], and diverged for etched particles (roughness to particle

59 diameter ratio = 0.6%) at a value of ϕ_{max} that is much lower than the maximum packing

60 expected for frictional particles ($\phi_{max} = 0.54$ [2]). We aim to present a general framework

61 that is relevant to colloids with shape anisotropy. Our results show that lubrication is

62 dominant in moderately concentrated suspensions. Tangential interactions become more

63 important at high shear rates, volume fractions, and surface roughness. A key observation

64 is that the onset stress for shear thickening is independent of ϕ only in the case of smooth

65 particles, and that roughness decreases this onset stress by reducing the force required to

66 push colloids into contact. We present the findings as a set of rheological state diagrams

67 that provide insight into the transition from shear thickening to dilatant flow for colloidal

68 suspensions.

69   We use density and refractive index-matched dispersions that contain poly(methyl

70 methacrylate) (PMMA) colloids with diameters $2a$ ranging from 1.9-2.8 μm [27-30], for

71 which flow occurs without inertia. The continuum phase is an organic solvent designed to

72 minimize sedimentation and van der Waals forces. A 10-nm layer of poly(12-

73 hydroxystearic acid) (PHSA) copolymer is grafted onto the colloids to provide a short-

74 range repulsive barrier against irreversible adhesion [28]. This steric stabilizer determines

75 the range and strength of the nearly hard sphere interactions of the colloids. Experimental

76 and numerical studies show that short-range steric stabilizers do not significantly alter the

77 strength of the shear thickening or dilatancy unless the solvent quality is drastically

78 changed [31-34]. Roughness of the colloids is tuned by varying the concentration of a

79 crosslinker. The crosslinker induces heterogeneity during oligomer precipitation,

80 resulting in size-monodisperse rough particles (**Fig. S1**, **Table S1**) [35]. Using this

81 method, we synthesize PMMA colloids with four types of asperities: smooth, slightly

82 rough (SL), medium rough (MR), and very rough (VR). These categories refer to

83 particles with different root-mean-square (RMS) roughness characterized using an atomic

4

84 force microscope (AFM) in tapping mode (**Fig. 1a**). The grafting length of the PHSA

85 brush is between 9% (VR colloids) to 50% (smooth colloids) of the RMS roughness. The

86 measured topography is fitted to a sphere with an effective radius, a_{eff}. The deviation of

87 surface profiles from a_{eff} is minimized by least squares fittings (**Fig. S2**). Volume

88 fractions are computed using a_{eff} values and from image volumes of particle suspensions

89 captured using confocal laser scanning microscopy (CLSM) [36]. We apply the relation ϕ

90 $= 4\pi a_{eff}{}^3 N_p/(3V_{box})$, where N_p is the total number of particles found in V_{box}, the total

91 volume of the CLSM image box analyzed. Our method of weighing particles and solvent

92 yields the correct value of ϕ to 2% (**Fig. S3**). An additional uncertainty in ϕ of 2% is

93 present due to particles swelling over time (**Fig. S4**). We characterize roughness using the

94 autocovariance of the topographic profile [37], $B(\psi) = \dfrac{1}{N} \displaystyle\sum_{\substack{i,j=1 \\ i \neq j}}^{\psi} \left(\left|\mathbf{r}_i\right| - a_{eff}\right)\left(\left|\mathbf{r}_j\right| - a_{eff}\right)$, where

95 N is the total number of data points analyzed and $\psi = \cos^{-1}\left(\dfrac{\mathbf{r}_i \cdot \mathbf{r}_j}{\left|\mathbf{r}_i\right|\left|\mathbf{r}_j\right|}\right)$ is the angle between

96 $\mathbf{r}_i$ and $\mathbf{r}_j$ as defined in **Fig. S2d**. The relative RMS roughness is expressed as $(B(\psi =$

97 $0)/a_{eff}{}^2)^{1/2}$ to account for different particle sizes. The full range of our experimental

98 conditions is in **Table S2**.

99 Colloids with large surface roughness shear thicken more readily. When vials

100 containing suspensions at $\phi = 0.52$ are inverted, smooth colloids flow like a viscous fluid

101 whereas rough colloids form finger-like structures (**Fig. S2**, **Movie S1**). To quantify the

102 shear thickening as a function of roughness and ϕ, we measure η and N_1 as a function of σ

103 in a stress-controlled rheometer. Performing stress sweeps up and down shows that the

104 flow is completely reversible for smooth colloids at $\phi = 0.55$, whereas MR colloids show

105   hysteresis in η and N_1 at $\phi = 0.535$ when steady state flow conditions are imposed (**Fig.**

106   **S5**). The hysteresis could be from geometric friction caused by interlocking particles

107   during flow. We also verify the absence of global slip by comparing the flow curve of

108   MR colloids with that collected with a different cone-and-plate geometry (**Fig. S6**).

109   **Fig. 1** shows the flow curves of the colloidal suspensions. At low σ, the

110   suspensions flow with a nearly constant relative viscosity, $\eta_{r,\mathrm{N}}$, defined as the quasi-

111   Newtonian plateau past the zero shear viscosity and the shear thinning regime [15]. As σ

112   increases, η begins to increase significantly at the onset of shear thickening. The critical

113   onset stress, σ_c, is the intersection of power laws fitted to the quasi-Newtonian and shear

114   thickening regimes (**Fig. 1b**). Smooth colloids undergo weak thickening in the range of ϕ

115   tested and progresses towards strong thickening when surface roughness increases.

116   Although σ_c is independent of ϕ for smooth colloids, σ_c decreases with increasing ϕ for

117   SL, MR, and VR colloids. These observations are markedly different from multiple

118   studies, which show that σ_c is typically constant in both regimes of CST and DST [6, 21,

119   38]. We address the rationale for the difference between smooth and rough particles later.

120   The sign of N_1 changes from negative to positive at large σ in strong thickening,

121   indicating the presence of dilatancy. Our measurements show that smooth colloids

122   display negative N_1 values consistently, whereas increasing the RMS roughness causes

123   the sign change to occur at lower ϕ for MR ($\phi = 0.535, 0.55$) and VR colloids ($\phi = 0.50$)

124   (**Fig. 1c**). Previous studies have attributed negative N_1 values and a mild increase in η to

125   the formation of hydroclusters [13]. More recently, positive N_1 values are attributed to a

126   breakdown of lubrication films [6, 18]. Here, our simulations support our inference that

127   roughness shifts the shear thickening-dilatancy transition because of an increase in the

128   interparticle friction coefficient, μ. **Fig. 2a, b** show results of dissipative particle

129   dynamics (DPD) simulations [16] on a suspension of spherical particles ($\phi = 0.535$) with

130   adjustable tangential interactions ranging from frictionless ($\mu = 0$) to frictional ($\mu = 1$).

131   The simulations utilize both lubrication hydrodynamics and friction to support

132   experimental observations that dilatancy and strong thickening are caused by tangential

133   interactions from particle asperities.

134   Two main points can be taken from **Fig. 2**. First, σ_c shifts to lower values as μ and

135   roughness increase (**Fig. 2c, d**). This observation supports our hypothesis that particle

136   roughness is directly connected to friction. Since the critical onset stress is related to the

137   pairwise force balance, this also suggests that tangential interactions reduce the critical

138   force required to push particles into load-bearing contact. Second, there is a

139   corresponding change in N_1 from negative to positive values as μ increases beyond a

140   critical value. This sign change occurs only when tangential interactions are significant

141   compared to hydrodynamics. We note that the value of σ_c does not correspond to the

142   onset stress of dilatancy.

143   A natural follow-up question is: how does roughness contribute to the mechanism

144   of the flow transitions? To address this question, we analyze the quasi-Newtonian

145   viscosity, the onset stresses, and the shear thickening power as functions of roughness.

146   **Fig. 3a** shows that $\eta_{r,N}$ diverges more rapidly with increasing ϕ for rougher particles. Our

147   data fit well to the empirical Eilers model $\eta_{r,N} = [1+1.5(1-\phi/\phi_{max})^{-1}]^2$, where ϕ_{max} is the

148   volume fraction at which the viscosity diverges [39, 40]. The $\eta_{r,N}$ data for smooth and SL

149   colloids fall within the spread measured in previous works [21, 26, 41, 42], whereas MR

150   and VR colloids differ significantly. This is not due to uncertainties in ϕ for the rough

151   colloids (**Fig. S3)**. Their lower values of ϕ_{max} imply that a rough particle occupies

152   excluded volumes larger than that of an equivalent ideal smooth sphere, especially in

153   flow regimes where contacts are minimal and particles fully rotate in the flow field. **Fig.**

154   **3b** plots ϕ_{max} as a function of roughness, along with values for smooth colloids from

155   literature. When roughness is greater than a specific length scale $(B(\psi = 0)/a_{eff}^2)^{1/2} \geq$

156   $0.07a_{eff}$), packing becomes increasingly difficult and hence the suspension viscosity

157   diverges at a value of ϕ_{max} below that of the maximum random close packing of ideal

158   spheres ($\phi_{max} = 0.64$). Interestingly, the value of ϕ_{max} for VR colloids ($\phi_{max} = 0.54$) is in

159   agreement with the maximum packing reported for frictional particles [2, 19].

160   **Fig. 3b** supports our hypothesis that the RMS roughness of particles needs to be

161   sufficiently large in order for frictional contacts to be generated. This is likely due to the

162   dissipative hydrodynamic forces from squeezing flow being diminished at a particle

163   separation of $h = 0.07a_{eff}$ (**Fig. S7**). An analogous transition from the hydrodynamic to

164   the boundary lubrication regime is well known in tribology [43] and granular packings.

165   Studies of granular packings support our observation that ϕ_{max} decreases with increasing

166   roughness, since frictional grains have a lower isostatic criterion [44].

167   **Fig. 3c** shows that as roughness increases, there is a corresponding increase in the

168   shear thickening power β. Based on our observations in **Fig. 3b**, we hypothesize that

169   tangential contributions from surface roughness can overcome the hydrodynamic forces

170   that keep particles apart in quasi-Newtonian flow and in weak thickening. We estimate

171   the force it takes to push two colloids into close contact using $F^* = \sigma_c a_{eff}^2$. It has been

172   shown that the threshold stress scaling is $\sigma_c \sim a_{eff}^2$ for sterically stabilized PMMA

173   particles, which comes from balancing the lubrication force and interparticle forces

174　between the cross sectional area of a particle pair [15, 21]. **Fig. 3d** shows that $F^* = 4.7$

175　k_BT/nm for smooth colloids at all ϕ/ϕ_{max}, consistent with the range of forces reported for

176　PHSA-PMMA particles ($F^* = 2.4 - 6.0$ k_BT/nm) [21, 45]. These units represent the energy

177　barrier that a pair of particles needs to overcome for a closer approach. Increasing surface

178　roughness decreases F^* by nearly an order of magnitude. Plotting F^* against ϕ/ϕ_{max} does

179　not collapse the data for different roughness, unlike studies in which the effect of

180　repulsive interactions on the flow curve can be collapsed [33]. This suggests that there

181　are other mechanisms in addition to packing effects during shear thickening and

182　dilatancy. While granular-like frictional interactions and force networks may be present

183　[46], elastohydrodynamic lubrication from particle deformation could also be present,

184　although deformation is expected to reduce the thickening strength [43]. The addition of

185　the crosslinker in our synthesis procedure can result in an increase in the elastic modulus

186　of PMMA by up to 40% at room temperature [47]. However, this change in modulus

187　cannot immediately explain the observation of positive N_1 values [16]. Although the

188　PHSA brush copolymer may entangle or adhere during flow [48, 49], direct force

189　measurements show that the interaction energy is purely repulsive down to a separation

190　distance of ~ 5 nm [50]. Thus, the observed shear thickening behavior and the switch in

191　the sign of N_1 from negative to positive is primarily due to the increasing roughness of

192　the colloids. Future studies incorporating the second normal stress difference, N_2, would

193　be necessary to fully characterize the hydrodynamic interactions in dense suspensions

194　[14, 26].

195　　　According to **Fig. 4**, lubrication dominates the quasi-Newtonian flow of

196　suspensions at low ϕ, σ, and roughness. When roughness increases, lubrication gradually

197 gives way to other microscopic mechanisms that generate tangential forces and lower the

198 critical stresses required for shear thickening and dilatancy. At the highest ϕ and σ, shear

199 thickening and dilatancy are present because interparticle forces become sufficiently

200 strong to deform particles [43] or press them into solid-solid contact [6]. In the case of

201 smooth colloids, the onset stress is constant up to $\phi = 0.55$. Roughness decreases the

202 onset stress in a similar way to frictional interactions in granular materials, in which the

203 microstructural criterion for mechanical stability is reduced [44, 51].

204 Because friction is a major factor in dense suspensions, our work provides a

205 guiding framework for predicting the rheology of a diverse class of colloidal materials

206 with anisotropic particle shapes that introduce a hindered rotation mechanism in shear

207 flow. Cornstarch is a particularly popular choice in studying jammed materials [19, 52,

208 53]. However, individual granules possess irregularly faceted surfaces [54]. Manipulation

209 of particle roughness and shape represents a powerful tool for which the desired

210 thickening response can be built into technology [55, 56]. Moreover, researchers working

211 on slurries can use particle roughness to minimize shear thickening or dilatancy.

References

[1] N. J. Wagner and J. F. Brady, *Phys. Today* **62**, 27 (2009).

[2] M. Wyart and M. E. Cates, *Phys. Rev. Lett.* **112**, 098302 (2014).

[3] Z. Pan, H. de Cagny, B. Weber, and D. Bonn, *Phys. Rev. E* **92**, 032202 (2015).

[4] V. T. O'Brien and M. E. Mackay, *Langmuir* **16**, 7931 (2000).

[5] E. Brown and H. M. Jaeger, *Rep. Prog. Phys.* **77**, 046602 (2014).

[6] J. R. Royer, D. L. Blair, and S. D. Hudson, *Phys. Rev. Lett.* **116**, 188301 (2016).

[7] O. Reynolds, *Philosophical Magazine Series 5* **20**, 469 (1885).

[8] M. Lee, M. Alcoutlabi, J. Magda, C. Dibble, M. Solomon, X. Shi, and G. McKenna, *J. Rheol.* **50**, 293 (2006).

[9] E. Brown and H. M. Jaeger, *J. Rheol.* **56**, 875 (2012).

[10] A. Fall, N. Huang, F. Bertrand, G. Ovarlez, and D. Bonn, *Phys. Rev. Lett.* **100**, 018301 (2008).

[11] X. Cheng, J. H. McCoy, J. N. Israelachvili, and I. Cohen, *Science* **333**, 1276 (2011).

[12] S. Jamali, M. Yamanoi, and J. Maia, *Soft Matter* **9**, 1506 (2013).

[13] D. R. Foss and J. F. Brady, *J. Fluid Mech.* **407**, 167 (2000).

[14] J. Bergenholtz, J. Brady, and M. Vicic, *J. Fluid Mech.* **456**, 239 (2002).

[15] J. Mewis and N. J. Wagner, *Colloidal Suspension Rheology* (Cambridge University Press, 2012).

[16] S. Jamali, A. Boromand, N. Wagner, and J. Maia, *J. Rheol.* **59**, 1377 (2015).

[17] A. K. Gurnon and N. J. Wagner, *J. Fluid Mech.* **769**, 242 (2015).

[18] R. Seto, R. Mari, J. F. Morris, and M. M. Denn, *Phys. Rev. Lett.* **111**, 218301 (2013).

[19] I. R. Peters, S. Majumdar, and H. M. Jaeger, *Nature* **532**, 214 (2016).

[20] N. Y. C. Lin, B. M. Guy, M. Hermes, C. Ness, J. Sun, W. C. K. Poon, and I. Cohen, *Phys. Rev. Lett.* **115**, 228304 (2015).

[21] B. M. Guy, M. Hermes, and W. C. K. Poon, *Phys. Rev. Lett.* **115**, 088304 (2015).

[22] N. Fernandez *et al.*, *Phys. Rev. Lett.* **111**, 108301 (2013).

[23] C. Heussinger, *Phys. Rev. E* **88**, 050201 (2013).

[24] R. Mari, R. Seto, J. F. Morris, and M. M. Denn, *J. Rheol.* **58**, 1693 (2014).

[25] D. Lootens, H. van Damme, Y. Hémar, and P. Hébraud, *Phys. Rev. Lett.* **95**, 268302 (2005).

[26] C. D. Cwalina and N. J. Wagner, *J. Rheol.* **58**, 949 (2014).

[27] L. Antl, J. Goodwin, R. Hill, R. H. Ottewill, S. Owens, S. Papworth, and J. Waters, *Colloids Surf.* **17**, 67 (1986).

[28] M. T. Elsesser and A. D. Hollingsworth, *Langmuir* **26**, 17989 (2010).

[29] L. Palangetic, K. Feldman, R. Schaller, R. Kalt, W. R. Caseri, and J. Vermant, *Faraday Discuss.* **191**, 325 (2016).

[30] L. C. Hsiao, R. S. Newman, S. C. Glotzer, and M. J. Solomon, *Proc. Natl. Acad. Sci. USA* **109**, 16029 (2012).

[31] J. Mewis and G. Biebaut, *J. Rheol.* **45**, 799 (2001).

[32] L.-N. Krishnamurthy, N. J. Wagner, and J. Mewis, *J. Rheol.* **49**, 1347 (2005).

[33] R. Mari, R. Seto, J. F. Morris, and M. M. Denn, *Proc. Natl. Acad. Sci. USA* **112**, 15326 (2015).

[34] S. Pednekar, J. Chun, and J. F. Morris, *Soft Matter* **13**, 1773 (2017).

258   [35] D. Kim, D. Y. Lee, K. Lee, and S. Choe, *Macromol. Res.* **17**, 250.

259   [36] W. C. K. Poon, E. R. Weeks, and C. P. Royall, *Soft Matter* **8**, 21 (2012).

260   [37] J. M. Bennett, *Appl. Opt.* **15**, 2705 (1976).

261   [38] B. J. Maranzano and N. J. Wagner, *J. Chem. Phys.* **114**, 10514 (2001).

262   [39] J. J. Stickel and R. L. Powell, *Annu. Rev. Fluid Mech.* **37**, 129 (2005).

263   [40] D. B. Genovese, *Adv. Colloid Interface Sci.* **171–172**, 1 (2012).

264   [41] S.-E. Phan, W. B. Russel, Z. Cheng, J. Zhu, P. M. Chaikin, J. H. Dunsmuir, and R.
265   H. Ottewill, *Phys. Rev. E* **54**, 6633 (1996).

266   [42] W. J. Frith, P. d'Haene, R. Buscall, and J. Mewis, *J. Rheol.* **40**, 531 (1996).

267   [43] G. Stachowiak and A. W. Batchelor, *Engineering Tribology* (Butterworth-
268   Heinemann, 2013).

269   [44] M. v. Hecke, *J. Phys. Condens. Matter* **22**, 033101 (2010).

270   [45] G. Bryant, S. R. Williams, L. Qian, I. K. Snook, E. Perez, and F. Pincet, *Phys. Rev.*
271   *E* **66**, 060501 (2002).

272   [46] D. Bi, J. Zhang, B. Chakraborty, and R. P. Behringer, *Nature* **480**, 355 (2011).

273   [47] K. Tamareselvy and F. A. Rueggeberg, *Dent. Mater.* **10**, 290 (1994).

274   [48] S. Auer, W. Poon, and D. Frenkel, *Phys. Rev. E* **67**, 020401 (2003).

275   [49] D. Cebula, J. Goodwin, R. H. Ottewill, G. Jenkin, and J. Tabony, *Coll. Polym. Sci.*
276   **261**, 555 (1983).

277   [50] B. Costello, P. Luckham, and T. F. Tadros, *Langmuir* **8**, 464 (1992).

278   [51] L. E. Silbert, *Soft Matter* **6**, 2918 (2010).

279   [52] A. Fall, F. Bertrand, D. Hautemayou, C. Mezière, P. Moucheront, A. Lemaître, and
280   G. Ovarlez, *Phys. Rev. Lett.* **114**, 098301 (2015).

281   [53] Y. Madraki, S. Hormozi, G. Ovarlez, E. Guazzelli, and O. Pouliquen, *Physical*
282   *Review Fluids* **2**, 033301 (2017).

283   [54] J. E. Fannon, R. J. Hauber, and J. N. BeMiller, *Cereal Chem.* **69**, 284 (1992).

284   [55] Y. S. Lee, E. D. Wetzel, and N. J. Wagner, *J. Mater. Sci.* **38**, 2825 (2003).

285   [56] E. Brown, N. Rodenberg, J. Amend, A. Mozeika, E. Steltz, M. R. Zakin, H. Lipson,
286   and H. M. Jaeger, *Proc. Natl. Acad. Sci. USA* **107**, 18809 (2010).

287

294   **Author contributions**

295   L.C.H. conceived and designed the study, synthesized and characterized the

296   colloidal particles, performed all experiments, analyzed data, and interpreted the results.

297   S.J. designed, ran, and analyzed the DPD simulations. D.B.V. analyzed roughness

298   parameters from AFM data collected by E.G. L.C.H., S.J., R.G.L. and M.J.S. analyzed

299   the results and wrote the manuscript. All authors commented on the manuscript.
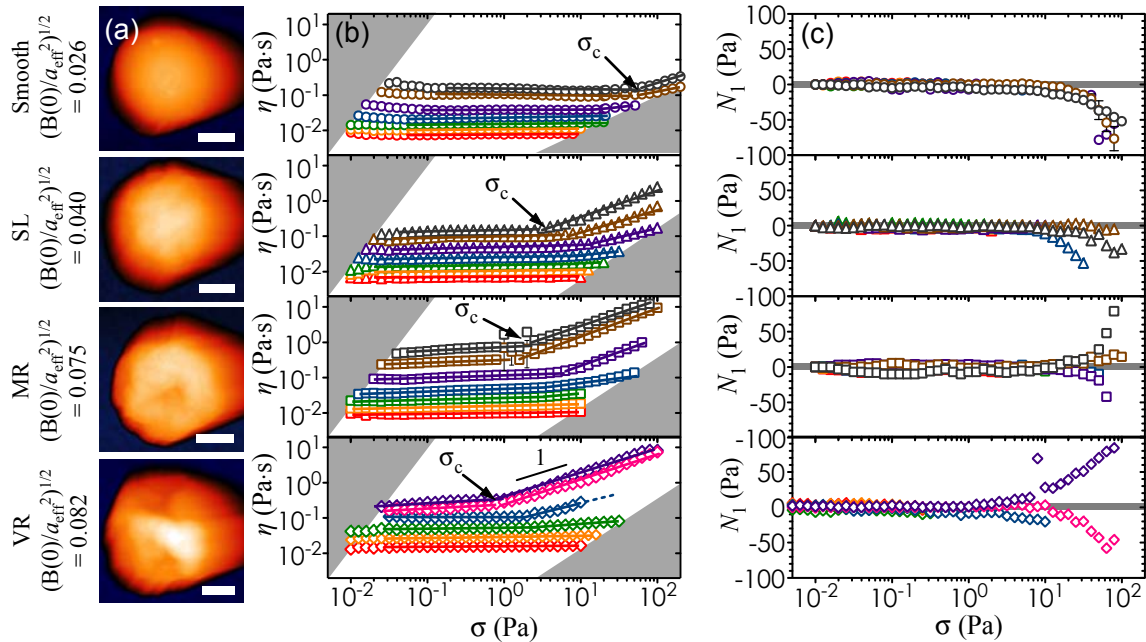
Figure 1 | Effect of particle roughness on suspension rheology. (a) Atomic force microscopy images of (top to bottom): smooth, SL, MR, and VR colloids. Scale bars = 1 μm. (b, c) Flow curves of suspensions consisting of these colloids (red, $\phi = 0.30$; orange, $\phi = 0.35$; green, $\phi = 0.40$; blue, $\phi = 0.45$; pink, $\phi = 0.48$; purple, $\phi = 0.50$; brown, $\phi = 0.535$; grey, $\phi = 0.55$). Solid lines are power law fits to the data. The data for VR colloids at $\phi = 0.45$ represent a limited stress range; a dashed line is extrapolated for visibility. Grey regions in (b) indicate instrument sensitivity limits on the left and inertial/fracture effects on the right, and grey regions in (c) centered about $N_1 = 0$ Pa indicate instrument limits. Error bars, where available, represent standard deviations from three independent upward stress sweeps.

14

311
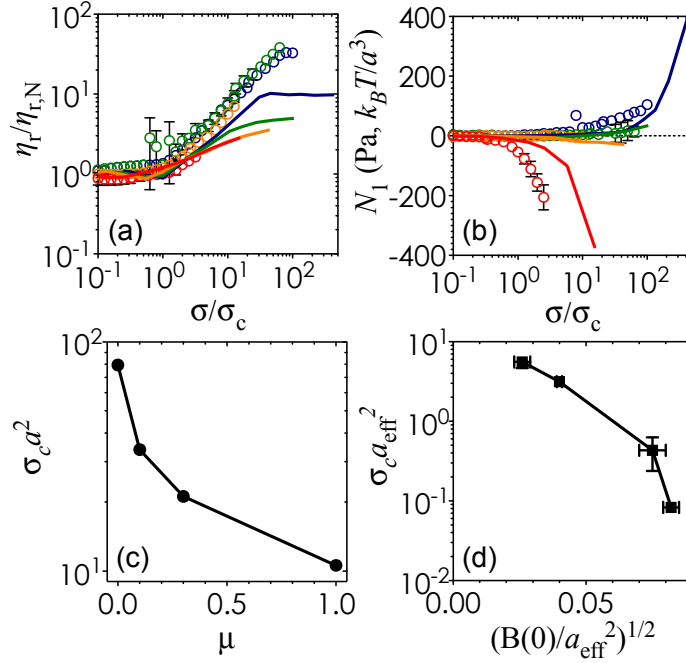
Figure 2 | Simulations and experiments of frictionless (smooth) and frictional (rough) particles. (a), Normalized steady state viscosity and (b), N_1 values of colloidal suspensions. Both plots are generated for $\phi = 0.535$ (except for VR colloids plotted at $\phi = 0.50$). Data from experiments are open circles for four types of roughness (smooth, red; SL, orange; MR, green; VR, blue) and data from DPD simulations are plotted as solid lines for DPD particles with varying friction coefficients ($\mu = 0$, red; $\mu = 0.1$, orange; $\mu = 0.3$, green; $\mu = 1$, blue). (c) The critical onset stress as a function of roughness in experiments and (d) as a function of μ in DPD simulations. Error bars represent standard deviations from three independent measurements.
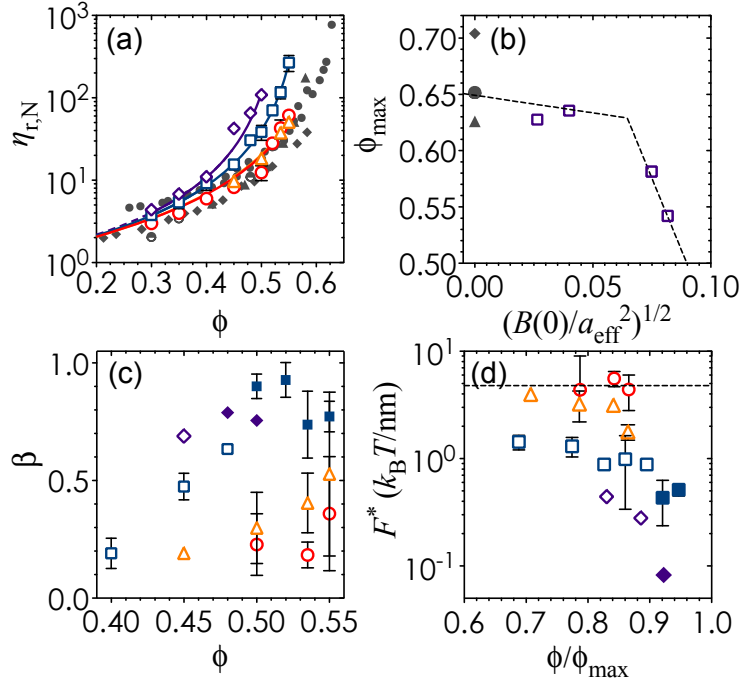
Figure 3 | Suspension properties as a function of roughness. (a), The relative quasi-Newtonian viscosity plotted against ϕ for smooth (red open circles), SL (orange open triangles), MR (blue open squares), and VR colloids (purple open diamonds). Solid lines are fits with the Eilers model. Grey filled symbols are literature data for sterically-stabilized PMMA [21, 41, 42] and silica colloids [26]. (b), Maximum packing fraction plotted against RMS roughness (open purple squares). Grey filled symbols are data of smooth colloids in literature [21, 26, 41, 42]. Dashed lines guide the eye. (c), Shear thickening power for different ϕ. (d), Onset force F^* to push particles into contact. Dashed line indicate constant F^* for smooth colloids. In (c) and (d) the symbols follow the same legend as in (a). Filled symbols indicate flow curves for dilatant samples. Error bars represent standard deviation from three independent measurements where available.

333
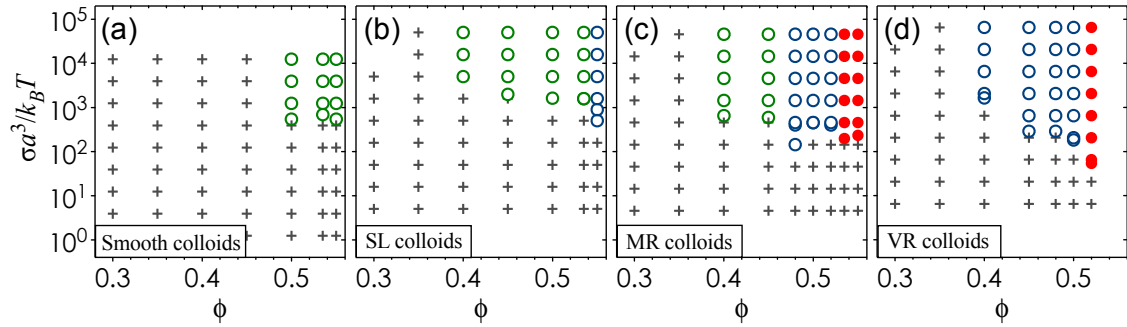
Figure 4 | Rheological state diagrams for rough colloids in sheared suspensions. (a-d), Transitions from quasi-Newtonian behavior to shear thickening and dilatancy are shown as a function of roughness. Grey crosses represent quasi-Newtonian flows ($\beta < 0.10$), green open circles represent weak thickening ($0.10 \leq \beta \leq 0.70$), blue open circles represent strong thickening ($0.70 \leq \beta \leq 1.0$), and red filled circles are dilatant flows ($N_1 > 0$).